Localization-delocalization transition in Hessian matrices of topologically disordered systems

B. J. Huang and Ten-Ming Wu*

Institute of Physics, National Chiao-Tung University, HsinChu, Taiwan 300, Republic of China

(Received 17 September 2007; revised manuscript received 12 November 2008; published 6 April 2009)

Using the level-spacing (LS) statistics, we have investigated the localization-delocalization transitions (LDTs) in Hessian matrices of a simple fluid with short-ranged interactions. The model fluid is a prototype of topologically disordered systems and its Hessian matrices are recognized as an ensemble of Euclidean random matrices with elements subject to several kinds of constraints. Two LDTs in the Hessian matrices are found, with one in the positive-eigenvalue branch and the other in the negative-eigenvalue one. The locations and the critical exponents of the two LDTs are estimated by the finite-size scaling for the second moments of the nearest-neighbor LS distributions. Within numerical errors, the two estimated critical exponents are almost coincident with each other and close to that of the Anderson model (AM) in three dimensions. The nearest-neighbor LS distribution at each LDT is examined to be in a good agreement with that of the AM at the critical disorder. We conclude that the LDTs in the Hessian matrices of topologically disordered systems exhibit the critical behaviors of orthogonal universality class.

DOI: 10.1103/PhysRevE.79.041105 PACS number(s): 61.25.Mv, 63.50.−x, 61.20.Ne

I. INTRODUCTION

The localization-delocalization transition (LDT) in disordered systems has attracted much attention since the pioneering work by Anderson [1] about localization. Investigation for the universality of the LDT remains one of the essential problems in condensed-matter physics [2,3]. Many universal properties about the LDT are obtained from the Anderson model (AM) for electron transport in a simple-cubic lattice with the on-site energies randomly distributed within a width W [4–8]. In dimension $d=3$, the on-site energy distribution has a critical width W_C so that the electron wave functions in the central region of the energy band are delocalized in space for $W<W_C$ and all wave functions become localized for $W>W_C$. The energy levels in these two regimes of disorder are described by different statistics: The nearest-neighbor level-spacing (LS) distribution of the delocalized states for $W<W_C$ is very close to the Wigner surmise $P_W(s)=(\pi/2)s\exp(-\pi s^2/4)$, while the distribution of the localized states for $W>W_C$ changes to the Poisson distribution $P_P(s)=\exp(-s)$, where s is the energy spacing between adjacent levels normalized by the mean LS. At $W=W_C$, the wave functions around the energy-band center behave in a multifractal nature [9], and the level statistics is characterized by a critical nearest-neighbor LS distribution $P_C(s)$, which is fundamentally different from $P_W(s)$ and $P_P(s)$. At small s, the behavior of $P_C(s)$ is accepted to be linear with a slope larger than that of the Wigner surmise and depending on the choice of the boundary conditions in the AM [10]. Numerical works suggest that $P_C(s)$ at large s is the Poisson-type with a decay rate above unity [5,7]; however, some analytical theory predicts other asymptotic behavior [11]. According to the scaling theory of localization [12], $P_C(s)$ is a scale-invariant function; this has been evidenced by numerical studies with the AM [7,13]. Based on this universal feature, the scale invariance of $P_C(s)$ provides a method to determine the LDTs in disordered systems other than for electron transport [14,15]. Compared with other approaches, this method benefits by only requiring the energy levels of a disordered system at several sizes; however, very large system sizes and a large amount of realizations for average have to be considered.

Recently, many efforts have been devoted to study harmonic vibrations in topologically disordered systems, which have no reference frame of lattice [16–22]. In harmonic approximation, vibrations in a topologically disordered system composed of particles of equal masses are described by the eigenmodes of its Hessian matrices, which are the second derivatives of potential energy of the system with respect to particle displacements and inversely weighted by the particle mass. In $d=3$, the Hessian matrices are composed of 3×3 blocks, which are functions of relative displacements of particle pairs [23,24], and can be recognized as a generalized version of the Euclidean random matrices [25], with randomness originated from the disorder of particle positions. From the viewpoint of the random matrix theory [26], Hessian matrices of topologically disordered systems fall into the same universality class with the AM. But the elements of each Hessian matrix are subject to constraints [27], which are classified into three categories: (I) the sum rules between the diagonal and off-diagonal blocks due to momentum conservation of the system, which makes the diagonal blocks determined by the off-diagonal ones; (II) the triangle rule for the relative positions of any three particles [28], which makes only $N-1$ off-diagonal blocks independent, with N being the particle number of the system, and (III) the internal constraints of each off-diagonal block, which reduce the degrees of freedom of an off-diagonal block to the three components of relative displacement of the related particle pair. None of these constraints appear in the AM. The triangle-rule constraints are not considered in those vibrational models with a lattice reference frame [29,30]. The constraints in (III) are ignored in the scalar-vibration models [31–34].

For topologically disordered systems in three-dimension space, the spectrum of harmonic vibrations can be separated into the extended (or delocalized) and localized regions: the

*tmw@faculty.nctu.edu.tw

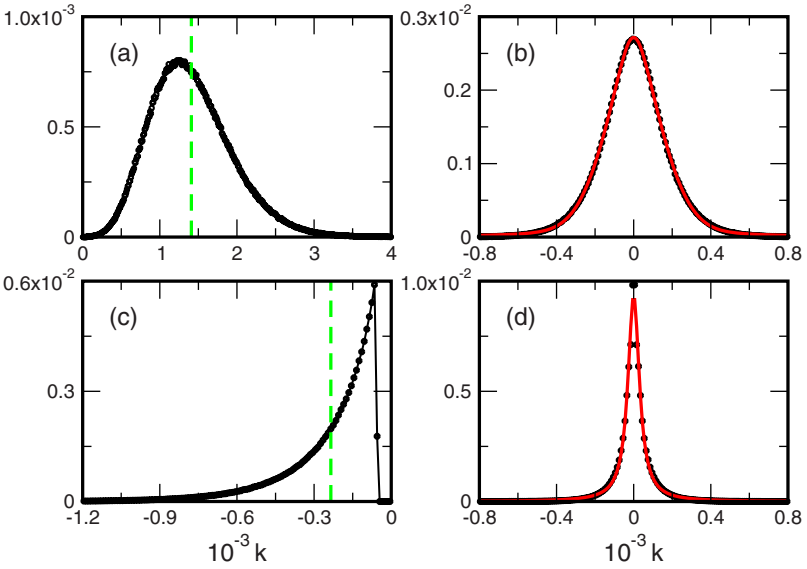

FIG. 1. (Color online) Normalized distributions of the elements in Hessian matrices of the TLJ fluid at $\rho^*=0.972$ and $T^*=0.836$: (a) for the traces of the diagonal blocks; (b) for the off-diagonal elements in the diagonal blocks; (c) for the traces of the off-diagonal blocks; and (d) for the off-diagonal elements in the off-diagonal blocks. In all figures, the abscissas are force constants in the units of ϵ/σ^2 and the symbols are the numerical data. The dashed lines in (a) and (c) indicate the averages of the distributions, which are $\bar{k}_{\rm tot}$ and $-\bar{k}$, respectively. The solid line in (b) is the fit result with a pseudo-Voigt function, and the line in (d) is that with a Lorentzian.

vibrational modes with eigenvalues near zero are generally delocalized in nature, while those in the end of the spectrum are usually found to be localized. Thus, the sharp boundaries that separate the localized and delocalized regions in a vibrational spectrum, usually termed as mobility edge (ME) [35], are examples of the LDT. Thermal conductivity in topologically disordered systems, such as glasses, is associated with the ME in their vibrational spectra [36]. To determine the location of the ME, several methods with different measures, including participation ratios [37,38], multifractal analysis [30], the LS statistics [39–42], and the diagonal elements of the resolvent matrix [43], have been studied. However, highly demanding in accuracy, the determination for the ME by numerical calculations is still a challenge problem.

In this paper, we investigate the MEs of the Hessian matrices of a truncated Lennard-Jones (TLJ) fluid, which is a prototype of topologically disordered systems, with the matrices evaluated at fluid configurations at a thermodynamic state of the fluid. The eigenmodes of the corresponding Hessian matrices are referred as the instantaneous normal modes (INMs) of the fluid [44], and the eigenvalue spectrum of the INMs is associated with the local-curvature distribution of the potential-energy surface of the system [45]. In Sec. II, the randomness of the elements in Hessian matrices of the TLJ fluid is described. In Sec. III, the second moments of the nearest-neighbor LS distributions in several intervals chosen from the extended region to the localized one are calculated for four system sizes. Then, we employ the approach of finite-size scaling to determine the MEs [46,47]. Two MEs, one with positive eigenvalue and the other with negative eigenvalue, are found in the INM-eigenvalue spectrum. The critical exponents of the two MEs are estimated. The nearest-neighbor LS distribution at each ME is examined to be in a good agreement with $P_C(s)$ obtained from the AM. Our conclusions are given in Sec. IV.

II. HESSIAN MATRICES OF THE TLJ FLUID

The TLJ potential $\phi_{\rm TLJ}(r)$ is obtained by truncating the Lennard-Jones (LJ) potential at the minimum $r_c=2^{1/6}\sigma$ and then lifting up in energy by ϵ [48], where σ and ϵ are the length and energy parameters of the LJ potential, respectively. So, the TLJ potential is purely repulsive. We choose the thermodynamic state of the TLJ fluid at reduced density $\rho^*=0.972$ and reduced temperature $T^*=0.836$ in the units of the two LJ parameters. With N particles confined in a cube of length $L=(N/\rho^*)^{1/3}$ and using the periodic boundary conditions, the fluid configurations are generated by Monte Carlo simulation for four system sizes from $N=3000$ to 24 000.

Owing to the short-range nature of the TLJ potential, the Hessian matrices are sparse. The ratio, $f_{\rm off}$, of the nonzero off-diagonal blocks in a Hessian matrix is estimated to be N_c/N, where N_c is the average number of neighbors around a particle within r_c. Evaluated by the radial distribution function of the TLJ fluid [49], N_c is about 6 and independent of N. Thus, $f_{\rm off}$ is inversely proportional to N, with a value about 0.05% for $N=12\,000$.

For each Hessian matrix, the trace of the off-diagonal block associated with particles i and j at distance r_{ij} is given by the negative of $k_{ij}=\phi''_{\rm TLJ}(r_{ij})+2\phi'_{\rm TLJ}(r_{ij})/r_{ij}$, where a prime stands for a derivative of the function. $\phi''_{\rm TLJ}(r_{ij})$ and $\phi'_{\rm TLJ}(r_{ij})/r_{ij}$ are, respectively, the force constants of the vibrational and rotational binary motions of the two particles [21]. The trace of the diagonal block associated with particle i, expressed as $\Sigma_{j\neq i}k_{ij}$, is the sum of all force constants connected to this particle. For the TLJ fluid, the traces of the diagonal and off-diagonal blocks are positive and negative values, respectively, and their averages, denoted as $\bar{k}_{\rm tot}$ and $-\bar{k}$, are related via the equation $\bar{k}_{\rm tot}=N_c\bar{k}$.

The randomness of the elements in the Hessian matrices can be described by four distributions: two for characterizing the traces and the off-diagonal elements of the diagonal blocks and the other two for the corresponding quantities of the off-diagonal blocks [50]. The four distributions of the TLJ fluid are shown in Fig. 1. Some features of the four distributions are given in the following: first, the distributions of the traces are asymmetric about their averages. Depending on the pair potential in the fluid, the distribution for the off-diagonal blocks has a sharp cusp, which is a result of

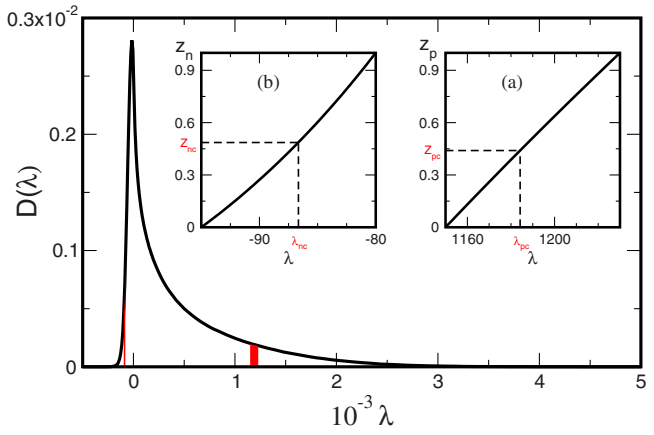

FIG. 2. (Color online) Normalized INM-eigenvalue spectrum, $D(\lambda)$, of the TLJ fluid at $\rho^*=0.972$ and $T^*=0.836$. λ is in unit of $\epsilon/m\sigma^2$, where m is the particle mass. The two insets show the unfolding procedures for the eigenvalues within the two shaded red regions in the main figure: (a) for λ between 1150 and 1230 and (b) for λ between -95 and -80. λ_{pc} and λ_{nc} are the locations of the MEs in the positive and negative branches, respectively.

the short-range nature of the TLJ potential [50]. Second, the distributions of the off-diagonal elements are symmetric about their averages, which are zero. The distribution for the off-diagonal blocks can be fit with a Lorentzian, reflecting the complete independence of the off-diagonal elements in the associated blocks. However, the distribution for the diagonal blocks can only be fit with a pseudo-Voigt function, which is a weighted linear combination of a Lorentzian and a Gaussian; the weighted factors of the Lorentzian and the Gaussian are about 40% and 60%, respectively. The reason why the pseudo-Voigt function is used is resulted from that the distribution is caused by a summation of the off-diagonal independent elements in the off-diagonal blocks and the number of the independent elements in the summation is about N_c, which is only a few in our model.

The Hessian matrices of the TLJ fluid are diagonalized with Lanczos method [51]. Presented in Fig. 2 is the normalized INM-eigenvalue spectrum $D(\lambda)$, which is an average for the realizations generated for each system size. Quite asymmetric with respect to the maximum at zero eigenvalue, the spectrum $D(\lambda)$ consists of two branches, one with positive eigenvalues and the other with negative eigenvalues. The physical meaning of the INMs with negative eigenvalues has been discussed in many literatures [52,53]. One ME is expected to occur in each branch. With the LS analysis given below for systems of smaller sizes [54], the MEs in $D(\lambda)$ are found within the range $\lambda=1150-1230$ and $\lambda=-95\sim-80$, which are the two shaded regions in Fig. 2.

III. MOBILITY EDGES IN THE INM-EIGENVALUE SPECTRUM

To do the LS analysis for eigenvalues from λ_1 to λ_2, we first unfold these eigenvalues λ_i with the following procedure [55]:

$$z_i = \frac{1}{D_0}\int_{\lambda_1}^{\lambda_i} D(\lambda)d\lambda, \tag{1}$$

where $D_0=\int_{\lambda_1}^{\lambda_2}D(\lambda)d\lambda$ is the percentage of the eigenvalues within the integral range. Shown in the insets of Fig. 2 are the unfolding procedures for the eigenvalues within the two shaded regions, with the unfolded eigenvalues z_p and z_n for the positive and negative branches, respectively. Since the function of $D(\lambda)$, although obtained numerically, is smooth enough, the unfolded eigenvalues are found to be uniformly distributed between zero and one.

For each branch, we select the unfolded eigenvalues in different sections, which have a width $\Delta z=0.125$ and are centered at $M\Delta z/2$ with M an integer from 1 to 15. For the unfolded eigenvalues z_i in a section, the nearest-neighbor LS is defined as $s_i=(z_{i+1}-z_i)/\Delta'$, where Δ' is the mean LS of the unfolded eigenvalues in this section. The LS data for the two shaded regions in Fig. 2 are summarized in Table I. The INM density of states in the shaded region in the positive branch is about four times smaller than that in the shaded region in the negative branch. Thus, for each system size, the number of samples in the calculation of the LS for the positive branch is four times of that for the negative branch; this makes the calculations for the positive branch much more difficult. The LS number of each section in the positive branch is about 2.2×10^6, and that of each section in the negative branch is about 3.8×10^5. For each section, we calculate the nearest-neighbor LS distribution $P(s)$, which is normalized and has a mean of unity. With the numerical $P(s)$ distribution of each section, the second moment I_N of $P(s)$, defined as $I_N=\int_0^\infty s^2P(s)ds$, is calculated. The data of I_N, including statistical errors, for the four system sizes we simu-

TABLE I. Numerical data of the LS statistics for the eigenvalues in the indicated ranges. N: number of particles; L: length of the simulated box in the LJ unit; M: number of samples; N_s: total number of LS; Δ: mean LS; $\Delta=(3ND_0)^{-1}$, where D_0 is the percentage of the eigenmodes in the range, equals to 1.54×10^{-2} and 1.06×10^{-2} for the positive and negative eigenvalues, respectively.

		λ from 1150 to 1230			λ from −95 to −80		
N	L	M	$N_s\times10^{-6}$	$\Delta\times10^3$	M	$N_s\times10^{-6}$	$\Delta\times10^3$
3000	14.56	128000	17.65	7.2	32000	3.020	10.5
6000	18.35	64000	17.65	3.6	16000	3.035	5.2
12000	23.12	32000	17.65	1.8	8000	3.042	2.6
24000	29.12	16000	17.65	0.9	4000	3.037	1.3

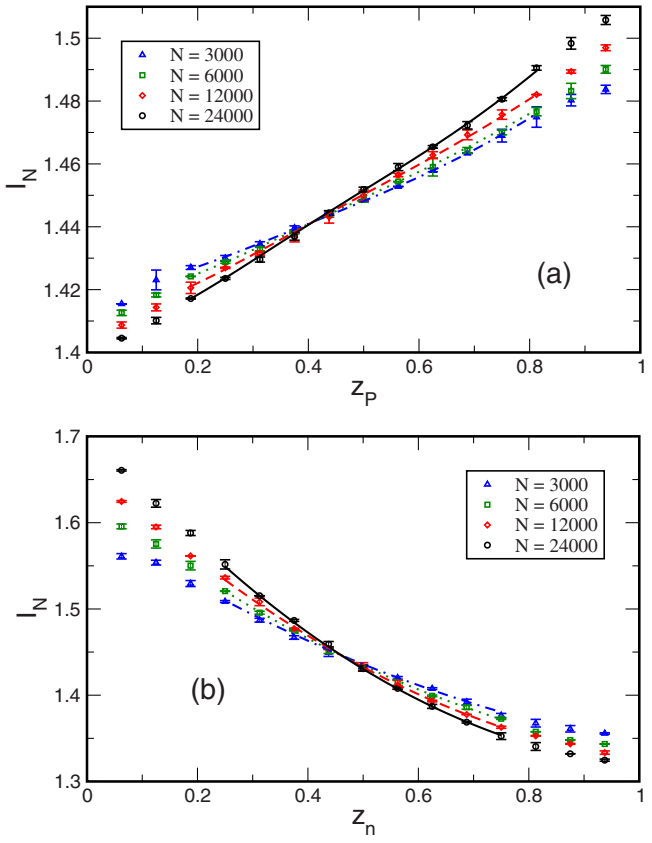

FIG. 3. (Color online) The second moment I_N of the LS distribution as a function of the unfolded eigenvalue: (a) for the positive branch and (b) for the negative branch. N is the number of particles in a system. The symbols (blue triangles for $N=3000$, green squares for $N=6000$, red diamonds for $N=12\,000$ and black circles for $N=24\,000$) are the results of the numerical eigenvalues obtained by diagonalization. The lines in (a) are the fitting functions of the model (1,0,3,3) for z_p within [0.1875,0.8125]; the lines in (b) are those of the model (0,0,2,2) for z_n within [0.25,0.75]; the solid, dashed, dotted and dot-dashed line styles are for $N=24\,000$, 12 000, 6000, and 3000, respectively.

lated are shown in Fig. 3. In principle, the values of I_N fall in a range between $4/\pi$ and 2, which are the second moments of the Wigner surmise and the Poisson distribution, respectively. For each system size, as the selected section moves from the delocalized to the localized region, the value of I_N increases monotonically. For each branch, the calculated I_N as a function of the unfolded eigenvalue z generally depends on system size and follows the scaling behavior: I_N increases with N in the localized region but decreases with N in the delocalized region. At some unfolded eigenvalue z_c, I_N is expected to be invariant with N and, therefore, z_c is the location of the ME in the branch.

A. Scaling near a ME

Each ME at z_c is expected to be characterized by the correlation length $\xi(z)$ of the infinite system. $\xi(z)$, which is a function of the unfolded eigenvalue z, diverges at z_c with a critical exponent ν and can be expressed as

$$\xi(z) = C|z - z_c|^{-\nu}, \tag{2}$$

where C is some constant. In order to extract the critical exponent from quantities X calculated for finite-size systems, one usually uses the one-parameter scaling hypothesis [12], in which X is a function of the form

$$X = f[L/\xi(z)]. \tag{3}$$

That is, after the system size L is scaled by $\xi(z)$, all quantities X of finite-size systems collapse onto a single scaling function.

For the data of I_N presented in Fig. 3, we make two kinds of corrections to the one-parameter scaling function. First, the scaling variable I_N apparently has a nonlinear dependence on the unfolded eigenvalue z. Second, for the possibility of a systematic shift of the crossing points of I_N curves, an irrelevant scaling variable is considered to appear in the scaling function. Once the system sizes are large enough, the systematic shift of the crossing points is expected to disappear so that the irrelevant scaling variable is not necessary. Thus, according to the renormalization theory for a critical point [46], we assume that the data of I_N obey the scaling law

$$I_N(z) = \tilde{f}(\chi_r L^{1/\nu}, \chi_i L^y), \tag{4}$$

where χ_r and χ_i are the relevant and irrelevant scaling variables with corresponding critical and irrelevant exponents ν and y, with $y<0$, respectively. Following the method given in Refs. [56,57], the $\tilde{f}$ function is expanded into a series of the irrelevant scaling variable up to order n_i:

$$I_N = \sum_{n=0}^{n_i} \chi_i^n L^{ny} \tilde{f}_n(\chi_r L^{1/\nu}), \tag{5}$$

and $\tilde{f}_n$ is also expanded into a series up to order n_r

$$\tilde{f}_n(\chi_r L^{1/\nu}) = \sum_{i=0}^{n_r} a_{ni} \chi_r^i L^{i/\nu}. \tag{6}$$

Due to the nonlinear dependence of the scaling variable I_N on z, χ_r, and χ_i are expanded into series up to order m_r and m_i, respectively,

$$\chi_r(Z) = \sum_{n=1}^{m_r} b_n Z^n, \quad \chi_i(Z) = \sum_{n=0}^{m_i} c_n Z^n, \tag{7}$$

where $Z=(z_c-z)/z_c$ and $b_1=c_0=1$. Each fitting function can be specified by a set of four indices (n_i,m_i,n_r,m_r) and the fitting parameters include those expansion coefficients, z_c, ν, and y. Of course, an appropriate fitting function should be the one with the total number of fitting parameters as few as possible.

We fit the I_N data within different intervals of z for the four system sizes with the scaling functions given in Eqs. (4)–(7). In a fit for N_d data points with a scaling function of N_p parameters, we use the downhill simplex method to minimize the χ^2 statistics of the data points, while the goodness of fit is measured by the Q factor, which is determined by the best-fit value of χ^2 and N_d-N_p, the number of degrees of freedom in the fitting [58]. In order to obtain the confidence

TABLE II. Fit parameters and estimates for z_{cp}, ν_p, and y_p with 95% confidence intervals for the positive branch. $z_{\min}$ and $z_{\max}$ give the fit interval of z. N_d is the number of data points in the interval. N_p is the number of fitting parameters. The value of χ^2 is for the best fit. Q is the goodness of fit. In each model, $m_i=0$.

$[z_{\min},z_{\max}]$	N_d	N_p	n_i	n_r	m_r	χ^2	Q	z_{cp}	ν_p	y_p
[0.25,0.75]	36	6	0	2	2	34.98	0.2435	0.433 ± 0.008	1.59 ± 0.08	0
[0.25,0.75]	36	7	0	2	3	35.43	0.1909	0.434 ± 0.008	1.60 ± 0.09	0
[0.25,0.75]	36	7	0	3	2	33.85	0.2449	0.428 ± 0.008	1.60 ± 0.09	0
[0.25,0.75]	36	8	0	3	3	31.69	0.2872	0.422 ± 0.010	1.52 ± 0.10	0
[0.25,0.75]	36	6	0	1	3	41.40	0.0804	0.435 ± 0.009	1.74 ± 0.07	0
[0.25,0.75]	36	6	0	3	1	49.29	0.0147	0.438 ± 0.009	1.79 ± 0.10	0
[0.1875,0.8125]	44	11	1	3	1	30.39	0.5978	0.431 ± 0.014	1.45 ± 0.09	-7.72 ± 5.32
[0.1875,0.8125]	44	11	1	3	3	25.92	0.7248	0.409 ± 0.017	1.54 ± 0.10	-6.00 ± 3.48

intervals of fit parameters, 10^4 synthetic data sets are generated by uniformly sampling each new data within the error bar of the data [57]. The error bars of fit parameters are estimated by those within 95% confidence intervals of its original fit. The acceptance of a fit is determined by two criteria. First, the Q value of an acceptable fit should be larger than 0.01 [58]. Second, since the value of ν is determined by the universality class of the random matrices, a large error of ν would make the fitting meaningless. So, we set the error bar of parameter ν for an acceptable fit to be less than 0.2. To keep the number of fit parameters as few as possible, we set $m_i=0$ for all fits and limit n_r and m_r no more than three. Also, verified by the results given below, no clear shift of the crossing points of the data curves in Fig. 3(b) is found so that, for the negative branch, the irrelevant scaling variable is not necessary and n_i is, therefore, set to be zero.

With the criterions given above, only several models are accepted for each branch, and the results are listed in Tables II and III. The distribution of the ν_p and ν_n values of the accepted models is shown in Fig. 4. For the negative branch, although the Q values of the accepted models are around 0.1, the fit values of z_{nc} and ν_n are generally close to one another, so we think all of these models are reliable. The average of these models leads us to $\nu_n=1.60\pm0.07$ and $z_{nc}=0.462\pm0.016$, which corresponds to $\lambda_{nc}=-87.1\pm0.3$. However, the accepted models for the positive branch are somewhat diversified. The two with ν_p larger than 1.7 have larger χ^2 values than others, causing their Q values less than 0.1. The rest four models without the irrelevant scaling variable have Q values generally more than 0.2 and their ν_p and z_{pc} values are close to one another. For the two models in which the irrelevant scaling variable is introduced, the goodness of fit substantially increases and the value of ν_p is relatively lowered; however, the value of irrelevant exponent y is large and its error is roughly the same order of y. By averaging the results of the six models with Q generally larger than 0.2, we have $\nu_p=1.55\pm0.09$ and $z_{pc}=0.426\pm0.011$, which gives $\lambda_{pc}=1183.8\pm0.8$.

In principle, ν_p and ν_n should coincide with each other, for the two MEs in the INM-eigenvalue spectrum belong to the same random matrices. On the other hand, due to the same universality class, the values of ν_p and ν_n should be equal to the critical exponent of the AM in $d=3$ [59,60]. Obtained by accurate numerical studies, the critical exponent of the AM in $d=3$ is reported to be 1.57 ± 0.02 [56]; however, other numerical studies give smaller values [57]. Within numerical errors, our results are generally satisfied with these requirements for ν_p and ν_n.

The solid lines in Fig. 3 present the fit results of the models with the highest Q value for each branch; the model of the positive branch is (1,0,3,3), in which the irrelevant scaling variable is used, and the one of the negative branch is

TABLE III. Fit parameters and estimates for z_{cn} and ν_n with 95% confidence intervals for the negative branch. The notations are the same meaning as those given in Table II. In each model, no irrelevant scaling variable is used, so $n_i=m_i=0$.

$[z_{\min},z_{\max}]$	N_d	N_p	n_r	m_r	χ^2	Q	z_{cn}	ν_n
[0.3125,0.6875]	28	6	1	3	31.91	0.0789	0.467 ± 0.061	1.63 ± 0.07
[0.3125,0.6875]	28	6	2	2	31.58	0.0848	0.464 ± 0.012	1.59 ± 0.10
[0.25,0.75]	36	6	2	2	39.13	0.1228	0.460 ± 0.007	1.60 ± 0.04
[0.3125,0.6875]	28	6	3	1	31.32	0.0897	0.461 ± 0.007	1.55 ± 0.09
[0.25,0.75]	36	6	3	1	39.19	0.1216	0.459 ± 0.005	1.60 ± 0.04
[0.3125,0.6875]	28	7	2	3	30.36	0.0851	0.465 ± 0.020	1.59 ± 0.09
[0.25,0.75]	36	7	2	3	39.09	0.1000	0.461 ± 0.009	1.60 ± 0.06
[0.25,0.75]	36	7	3	2	39.13	0.0992	0.460 ± 0.009	1.60 ± 0.04
[0.25,0.75]	36	8	3	3	38.98	0.0812	0.457 ± 0.016	1.63 ± 0.09

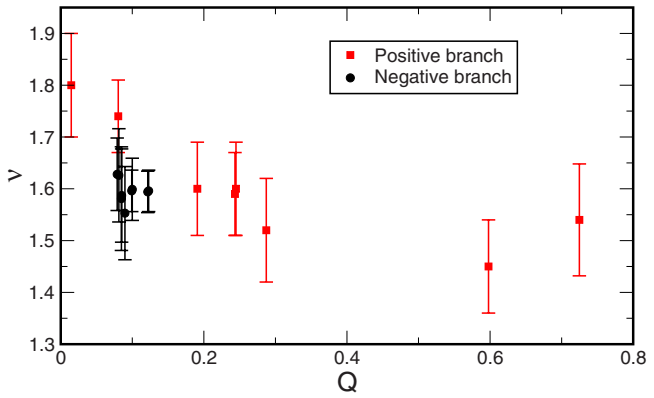

FIG. 4. (Color online) Fit values of the critical exponents with 95% confidence intervals as a function of Q. The red squares and black circles are for the models listed in Tables II and III for the positive and negative branches, respectively.

(0,0,2,2). The correlation length $\xi(z)$ of each ME can be given as $\xi_0|\chi_r(Z)|^{-\nu}$, where ν is the estimated value of ν_p or ν_n and ξ_0 is a constant but different for the two branches, and the correlation lengths of the two MEs are plotted in the insets of Fig. 5. For each branch, after the system sizes are scaled by the corresponding correlation length $\xi(z)$, the I_N data of the four system sizes collapse onto a single scaling function, which is shown in Fig. 5. One should notice that the I_N data shown in Fig. 5(a) have been corrected by the formula [56]

$$I_N^{\text{corr}} = I_N - L^y \tilde{f}_1(\chi_r L^{1/\nu}). \tag{8}$$

The scaling function consists of two continuous curves, separated by the value of I_N at the ME. Although the I_N values at the ME shown in Fig. 5 are slightly different for the two branches, the difference is within the error bars of the two I_N values. The upper and lower curves of the scaling function correspond to the localized and extended INMs, respectively. Thus, we have confirmed the scaling hypothesis for the INMs near each ME and suggest that the MEs in the INM-eigenvalue spectrum should follow the universality for the orthogonal random matrices.

B. $P(s)$ at each ME

To examine the critical behavior at the two MEs, we select two narrow intervals $\lambda = 1181.8 - 1185.8$ and $\lambda = -88.1 - -86.1$, which contain the MEs in the positive and negative branches, respectively. For the realizations of each system size generated by our simulations, the number of the LSs within the interval in the positive branch is about 8.9×10^5 and that within the interval in the negative branch is 4.1×10^5. Calculated for the four system sizes, the numerical data of the $P(s)$ distribution within each interval are presented by symbols with error bars in Fig. 6. Since the widths of the two selected intervals are small enough, the two $P(s)$ distributions, within numerical errors, are generally independent of system size N. We fit the $P(s)$ data of the four system sizes for s less than three by the following formula, which has used to fit the critical LS distribution of the AM [7],

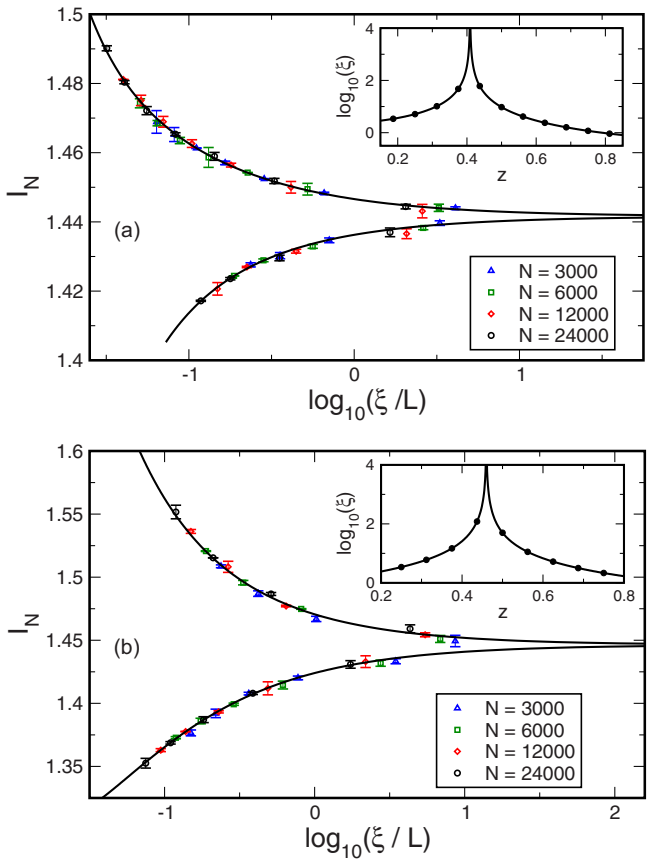

FIG. 5. (Color online) Scaling functions (solid line) of (a) the model (1,0,3,3) for the positive branch and (b) the model (0,0,2,2) for the negative branch. The symbols, with the same meaning as in Fig. 3, are the numerical data. The scaled I_N values in (a) have been corrected by Eq. (8); those in (b) are the original ones. The insets show the correlation lengths $\xi(z)$ near the two MEs.

$$P_C(s) = \frac{A_c^2 s}{\sqrt{\mu^2 + (A_c s)^2}} \exp[\mu - \sqrt{\mu^2 + (A_c s)^2}], \tag{9}$$

where A_c and μ are two fitting parameters. The normalized distribution in Eq. (9) has a linear behavior at small s with slope $P_C'(0) = A_c^2/\mu$ but changes to a Poisson-type form at large s with a decay rate A_c. Also, the second moment I_c of the distribution is given as $2(\mu+1)/A_c^2$.

Our results give $A_c = 1.89 \pm 0.02$ and $\mu = 1.565 \pm 0.015$ with the goodness of fit $Q = 0.69$ for the positive branch and $A_c = 1.9 \pm 0.02$ and $\mu = 1.568 \pm 0.020$ with Q close to one for the negative branch, where the errors of the fit parameters are estimated within 95% confidence interval. The numerical results and the fit for large s are shown in the insets of Fig. 6. Indicated by the fit data, the $P(s)$ distributions within the two selected intervals almost coincide with each other and the two values of A_c are almost the same as that of the AM [13]. Calculated with the values of A_c and μ, the slope $P_C'(0)$ at $s = 0$ has a value about 2.29, which is comparable with that of the AM with the periodic boundary conditions [10]. Similarly, the second moments I_c of the two fit distributions are close to 1.43, which is once again very close to the corresponding value of the AM. Thus, we have verified that,

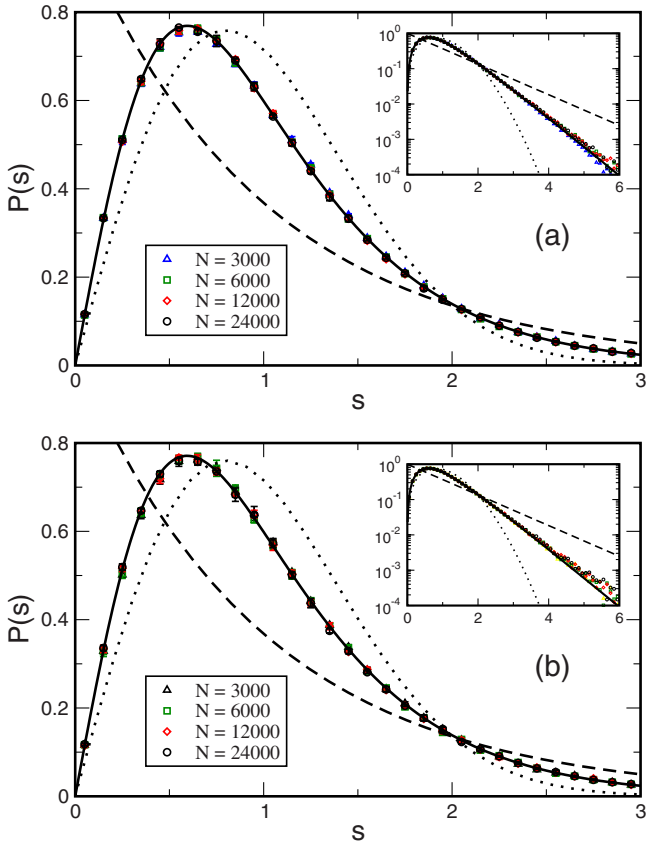

FIG. 6. (Color online) The nearest-neighbor LS distribution near the ME (a) in the positive branch or (b) in the negative branch. The symbols with error bars are the numerical data for the four system sizes, with the same symbol style as in Fig. 3 for each size. In each panel, the solid line represents the fit result with Eq. (9). The dotted and dashed lines are the Wigner surmise and the Poisson distribution, respectively. The insets show the large-s behavior of the distributions.

within numerical errors, the nearest-neighbor LS distribution near any ME in the INM spectrum of the TLJ fluid agrees the critical $P_C(s)$ distribution obtained from the AM, which supports the universality of the critical nearest-neighbor LS distribution.

IV. CONCLUSIONS

In this paper, we have performed LS analysis for Hessian matrices of the TLJ fluid at a thermodynamic state to investigate the properties of the LDT in topologically disordered systems, which have no reference frame of lattice. With disorder originated from the randomness of particle positions in the fluid, the Hessian matrices evaluated at the fluid configurations are an ensemble of Euclidean random matrices with elements subject to several constraints, and the matrices are sparse due to the short-range nature of the TLJ potential. By referring the eigenmodes of the matrices as the INMs, the eigenvalue spectrum of the INMs is composed of two branches corresponding to the positive and negative eigenvalues.

Calculated for four system sizes of the TLJ fluid and averaged for very large amounts of fluid configurations, the second moments of the nearest-neighbor LS distributions of the INMs within some small intervals in each branch are found to follow the scaling behavior near a LDT. In terms of the size invariance of the second moments, two LDTs, referred as the MEs, are confirmed to exist in the INM-eigenvalue spectrum, with one in the positive branch and the other in the negative branch. We have used the finite-size scaling to estimate the locations and the critical exponents of the two MEs. In the models to fit the data of the second moments, the nonlinear dependence of the scaling variable on the eigenvalue has been considered and an irrelevant scaling variable due to the finite-size effect is introduced in some models for the positive branch. In principle, the critical exponents of the two MEs should coincide in value; through the fitting, their values are found to be 1.55 ± 0.09 and 1.60 ± 0.07 for the positive and negative branches, respectively. Within numerical errors, the estimated values of the two critical exponents are almost coincident with each other and compatible with that of the AM in three dimensions [56]. The nearest-neighbor LS distributions at the two MEs are examined to be almost the same as the critical LS distribution obtained from the AM. Thus, we conclude that the MEs in the eigenvalue spectra of Hessian matrices of topologically disordered systems follow the universality for the orthogonal universality class and have nothing to do with the topological nature of the disorder in the systems and the constraints imposed on the Hessian matrices due to structural considerations.

ACKNOWLEDGMENTS

We acknowledge Professor R. A. Römer for helpful discussions and S. L. Chang for helping in computer calculations. T.M.W. acknowledges support from the National Science Council of Taiwan under Grant No. NSC 97-2112-M-009-005-MY2.

[1] P. W. Anderson, Phys. Rev. **109**, 1492 (1958).
[2] M. Janssen, Phys. Rep. **295**, 1 (1998).
[3] A. D. Mirlin, Phys. Rep. **326**, 259 (2000).
[4] A. MacKinnon and B. Kramer, Phys. Rev. Lett. **47**, 1546 (1981).
[5] B. I. Shklovskii, B. Shapiro, B. R. Sears, P. Lambrianides, and H. B. Shore, Phys. Rev. B **47**, 11487 (1993).
[6] E. Hofstetter and M. Schreiber, Phys. Rev. B **48**, 16979 (1993); Phys. Rev. B **49**, 14726 (1994).
[7] I. Kh. Zharekeshev and B. Kramer, Phys. Rev. Lett. **79**, 717 (1997).
[8] A. M. Garcia-Garcia and E. Cuevas, Phys. Rev. B **75**, 174203

(2007).
[9] M. Schreiber and H. Grussbach, Phys. Rev. Lett. **67**, 607 (1991).
[10] D. Braun, G. Montambaux, and M. Pascaud, Phys. Rev. Lett. **81**, 1062 (1998).
[11] A. G. Aronov, V. E. Kravtsov, and I. V. Lerner, JETP Lett. **59**, 39 (1994).
[12] E. Abrahams, P. W. Anderson, D. C. Licciardello, and T. V. Ramakrishnan, Phys. Rev. Lett. **42**, 673 (1979).
[13] I. Kh. Zharekeshev and B. Kramer, Jpn. J. Appl. Phys. **34**, 4361 (1995).
[14] C. P. Zhu and S. J. Xiong, Phys. Rev. B **62**, 14780 (2000).
[15] M. Sade, T. Kalisky, S. Havlin, and R. Berkovits, Phys. Rev. E **72**, 066123 (2005).
[16] T. S. Grigera, V. Martin-Mayor, G. Parisi, and P. Verrocchio, Phys. Rev. Lett. **87**, 085502 (2001).
[17] V. Martin-Mayor, M. Mèzard, G. Parisi, and P. Verrocchio, J. Chem. Phys. **114**, 8068 (2001).
[18] T. S. Grigera, V. Martin-Mayor, G. Parisi, and P. Verrocchio, Nature (London) **422**, 289 (2003).
[19] S. Ciliberti, T. S. Grigera, V. Martin-Mayor, G. Parisi, and P. Verrocchio, J. Chem. Phys. **119**, 8577 (2003).
[20] J. J. Ludlam, S. N. Taraskin, S. R. Elliott, and D. A. Drabold, J. Phys.: Condens. Matter **17**, L321 (2005).
[21] T. M. Wu, S. L. Chang, and K. H. Tsai, J. Chem. Phys. **122**, 204501 (2005).
[22] S. Ciliberti, P. De Los Rios, and F. Piazza, Phys. Rev. Lett. **96**, 198103 (2006).
[23] T. M. Wu and R. F. Loring, J. Chem. Phys. **97**, 8568 (1992).
[24] Y. Wan and R. M. Stratt, J. Chem. Phys. **100**, 5123 (1994).
[25] M. Mèzard, G. Parisi, and A. Zee, Nucl. Phys. B **559**, 689 (1999).
[26] M. L. Mehta, *Random Matrices* (Academic, San Diego, 1991).
[27] W. J. Ma, T. M. Wu, and J. Hsieh, J. Phys. A **36**, 1451 (2003).
[28] D. A. Parshin and H. R. Schober, Phys. Rev. B **57**, 10232 (1998).
[29] S. N. Taraskin, Y. L. Loh, G. Natarajan, and S. R. Elliott, Phys. Rev. Lett. **86**, 1255 (2001).
[30] J. J. Ludlam, S. N. Taraskin, and S. R. Elliott, Phys. Rev. B **67**, 132203 (2003).
[31] W. Schirmacher, G. Diezemann, and C. Ganter, Phys. Rev. Lett. **81**, 136 (1998).
[32] Y. Akita and T. Ohtsuki, J. Phys. Soc. Jpn. **67**, 2954 (1998).
[33] J. W. Kantelhardt, S. Russ, and A. Bunde, Phys. Rev. B **63**, 064302 (2001).
[34] S. N. Taraskin and S. R. Elliott, Phys. Rev. B **65**, 052201 (2002).
[35] S. Alexander and R. Orbach, J. Phys. (Paris), Lett. **43**, L625 (1982).
[36] P. B. Allen and J. L. Feldman, Phys. Rev. B **48**, 12581 (1993).
[37] W. Garber, F. M. Tangerman, P. B. Allen, and J. L. Feldman, Philos. Mag. Lett. **81**, 433 (2001).
[38] J. L. Feldman and N. Bernstein, Phys. Rev. B **70**, 235214 (2004).
[39] J. W. Kantelhardt, A. Bunde, and L. Schweitzer, Phys. Rev. Lett. **81**, 4907 (1998).
[40] P. Carpena and P. Bernaola-Galvan, Phys. Rev. B **60**, 201 (1999).
[41] S. Sastry, N. Deo, and S. Franz, Phys. Rev. E **64**, 016305 (2001).
[42] S. Ciliberti and T. S. Grigera, Phys. Rev. E **70**, 061502 (2004).
[43] S. Ciliberti, T. S. Grigera, V. Martin-Mayor, G. Parisi, and P. Verrocchio, Phys. Rev. B **71**, 153104 (2005).
[44] R. M. Stratt, Acc. Chem. Res. **28**, 201 (1995).
[45] T. Keyes, J. Phys. Chem. A **101**, 2921 (1997).
[46] J. Cardy, *Scaling and Renormalization in Statistical Physics* (Cambridge University Press, Cambridge, 1996).
[47] A. MacKinnon and B. Kramer, Z. Phys. B: Condens. Matter **53**, 1 (1983).
[48] T. M. Wu, W. J. Ma, and S. L. Chang, J. Chem. Phys. **113**, 274 (2000).
[49] T. M. Wu, W. J. Ma, and S. F. Tsay, Physica A **254**, 257 (1998).
[50] S. N. Taraskin and S. R. Elliott, J. Phys.: Condens. Matter **14**, 3143 (2002).
[51] J. K. Cullum and R. K. Willoughby, *Lanczos Algorithms for Large Symmetric Eigenvalue Computations* (Birkhauser, Boston, 1985).
[52] B. Madan and T. Keyes, J. Chem. Phys. **98**, 3342 (1993).
[53] H. E. Stanley, S. V. Buldyrev, N. Giovambattista, E. La Nave, M. Mossa, A. Scala, F. Sciortino, F. W. Starr, and M. Yamada, J. Stat. Phys. **110**, 1039 (2003) and references therein.
[54] We have performed the LS analysis given in the text for system sizes $N=375$, 750, and 1500.
[55] T. Guhr, A. Muller-Groeling, and H. A. Weidenmuller, Phys. Rep. **299**, 189 (1998).
[56] K. Slevin and T. Ohtsuki, Phys. Rev. Lett. **82**, 382 (1999).
[57] F. Milde, R. A. Römer, and M. Schreiber, Phys. Rev. B **61**, 6028 (2000).
[58] W. H. Press, B. P. Flannery, S. A. Teukolsky, and W. T. Vetterling, *Numerical Recipes in FORTRAN* (Cambridge University Press, Cambridge, 1989).
[59] I. V. Plyushchay, R. A. Römer, and M. Schreiber, Phys. Rev. B **68**, 064201 (2003).
[60] A. Eilmes, A. M. Fischer, and R. A. Römer, Phys. Rev. B **77**, 245117 (2008).